ROYAL SOCIETY
OF CHEMISTRY

Check for updates

Assessing the limitations of transparent conducting oxides as thermoelectrics†

Kieran B. Spooner, [ID] [ab] Alex M. Ganose [ID] ‡[ab] and David O. Scanlon [ID] ★[abc]

Thermoelectrics are a promising technology for converting heat into renewable electricity. Currently, however, most of the best thermoelectrics are based on toxic and/or rare materials such as PbTe and Bi_2Te_3, limiting their practical applications. Transparent conducting oxides (TCOs) are well understood and widely used commercially, so if they could be made into thermoelectrics, they could be rapidly and prolifically deployed. TCOs have been tested for their thermoelectric capabilities, however their performance is far below that needed for industrial deployment. Here we use hybrid density functional theory to screen four TCOs: $BaSnO_3$, CdO, SnO_2 and ZnO for thermoelectric efficiency and analyse the limitations of TCOs as thermoelectrics. We demonstrate that the dominant factor limiting these materials is the lattice thermal conductivity, and more specifically very long phonon mean free paths up to the order 10 μm, making them strong candidates for nanostructuring to increase performance. Based on these insights we critically discuss materials design principles for increasing the *ZT* of the conducting oxides.

1 Introduction

Despite the primary global energy consumption of around 160 PW h this decade[1,2] and the numerous negative effects this will bring,[3] an estimated 50% of all generated energy is wasted as heat.[4] One fifth of this wasted heat is theoretically recoverable,[4] and that recovery could reduce the effects of global heating in at least three ways: reducing energy consumption, generating emissions-free electricity and reducing the local increase of temperatures in urban areas caused in part by anthropogenic waste heat (the urban heat island effect)[5] by utilising some of said heat. Thermoelectrics, materials which transform heat into electricity (or *vice versa*), are promising candidates for this task.

The efficiency of a thermoelectric material is quantified by the dimensionless figure of merit, *ZT*:

$$ZT = \frac{\alpha^2 \sigma T}{\kappa} \quad \text{where } \kappa = \kappa_e + \kappa_l \tag{1}$$

where α is the Seebeck coefficient, σ is electrical conductivity, T is the absolute temperature and κ_e and κ_l are the electronic and lattice contributions to the thermal conductivity, κ, respectively.

ªDepartment of Chemistry, University College London, 20 Gordon Street, London, WC1H 0AJ, UK. E-mail: d.scanlon@ucl.ac.uk

ᵇThomas Young Centre, University College London, Gower Street, London WC1E 6BT, UK

ᶜDiamond Light Source Ltd., Diamond House, Harwell Science and Innovation Campus, Didcot, Oxfordshire OX11 0DE, UK

† Electronic supplementary information (ESI) available. See DOI: 10.1039/d0ta02247k

‡ Lawrence Berkeley National Laboratory, Energy Technologies, Area, 1 Cyclotron Road, Berkeley, CA 94720, USA.

The Seebeck coefficient quantifies the Seebeck effect,[6] the thermal diffusion of charge carriers from the hot to the cold end of a material, which results in a potential difference if there is an imbalance of electrons and their positive counterparts, holes. A high Seebeck coefficient requires a low number of poorly mobile charge carriers:

$$\alpha = \frac{\Delta V}{\Delta T} = \frac{2k_B^2 m^* T}{3e\hbar^2}\left(\frac{\pi}{3n}\right)^{\frac{2}{3}} \tag{2}$$

where V is the voltage, k_B is the Boltzmann constant, m^* is the charge carrier effective mass, e is the charge of an electron, $\hbar$ is the reduced Planck's constant and n is the charge carrier concentration. However, a high electrical conductivity requires large numbers of highly mobile charge carriers:

$$\sigma = ne\mu = \frac{ne^2\tau}{m^*} \tag{3}$$

where μ is the charge carrier mobility and τ is the charge carrier lifetime. Furthermore, charge carriers conduct heat as well as electricity, so a high electrical conductivity implies a high electronic component of the thermal conductivity:[7]

$$\kappa_e = L\sigma T \tag{4}$$

where L is the Lorenz number. While this will decrease *ZT*, thermoelectric design commonly employs the phonon-glass electron-crystal (PGEC) concept,[8] where the electronic thermal conductivity is allowed to be high in the interests of a high electrical conductivity, and instead the lattice thermal conductivity is minimised. The lattice thermal conductivity is carried by phonons, the quanta of lattice vibrations, which is commonly minimised in complex structures where there are

not long paths of similar atoms along which phonons can easily conduct.

While not a property intrinsic to a material, temperature is also an important factor in thermoelectric efficiency, as the ZT (eqn (1)) and Seebeck coefficient (eqn (2)) are both proportional to temperature. In addition, in semiconductors, higher temperatures excite more charge carriers, which can then conduct electricity, causing electrical conductivity to increase. There are also increased lattice vibrations, which impede the phonons that are conducting heat, reducing the lattice thermal conductivity. Therefore, and as evidenced by the data in Table 1, ZT tends to be higher at high temperatures. Furthermore, whilst waste heat at temperatures above 573 K makes up only 5.3% of the total across all temperatures, 17.4% of the theoretically recoverable energy came from these temperatures in 2014,[4] due to the steeper temperature gradients granting a higher Carnot efficiency.[15,16] This means that the recoverable energy from high temperature sources is much more concentrated than low temperature sources: for comparison, 31.3% of waste heat was from sources in the range 373–573 K, providing 62.7% of the theoretically recoverable energy, so while 3.6 times more heat can be recovered from sources in the lower temperature range, almost 6 times as much material would be required to access all the extra sources.[4] Oxide thermoelectrics,[17] with their high temperature stability (Table 2), are well placed to take advantage of these factors.

Transparent conducting oxides (TCOs) are a class of oxides that could be especially interesting. Unlike many oxides, they are electrically conductive, one of the qualities required for efficient thermoelectric materials. Furthermore, unlike many high efficiency thermoelectrics (Table 1), there are many TCOs which do not contain toxic elements such as Pb, which has lead to them being able to be used pervasively in the consumer market, especially in touchscreen and photovoltaic devices. Because of this they are extremely well understood, and could have an accelerated route to widespread deployment if they were able to be made into efficient thermoelectrics. TCOs have previously been studied experimentally for thermoelectric applications, especially ZnO, commonly in the form of Al doped ZnO (AZO),[21] which has so far achieved a ZT of over 0.1 at 300 K,[22] and if codoped with Ga it can reach 0.65 at 1000 K[23] (the record ZT for a singly doped TCO is 0.45 at 1273 K for $In_{1.8}Ge_{0.2}O_3$).[24] Although many experimental studies have tried various means of raising the thermoelectric efficiency of AZO, including changing synthesis conditions,[22,25–27] microstructure,[28] temperature and magnetic field,[29] doping[23,30–35] and

Table 1 Some $ZT \geq 2$ materials, representing the most efficient thermoelectrics so far discovered. All but $AgPb_{18}SbTe_{20}$ are p-type

Material	T (K)	ZT
$AgPb_{18}SbTe_{20}$ (ref. 9) (n-type)	800	2.2
PbTe–SrTe[10]	915	2.2
$PbTe_{0.86}Se_{0.07}S_{0.07}$:Na[11]	825	2.0
SnSe[12]	923	2.6
$Pb_{0.7}S_{0.3}$:K[13]	923	2.2
$PbTe_{0.8}Se_{0.2}$:MgTe[14]	820	2.2

Table 2 Melting or decomposition temperatures of $BaSnO_3$, CdO, SnO_2 and ZnO

Material	$BaSnO_3$	CdO	SnO_2	ZnO
T (K)	2138 (ref. 18)	1473 (ref. 19)	1903 (ref. 20)	2247 (ref. 20)

nanostructure;[36] a study of the limitations of TCOs as thermoelectrics has not, to the authors' knowledge, been conducted. Here we screen the TCOs $BaSnO_3$, CdO, SnO_2 and ZnO for thermoelectric applications in order to assess their efficiencies, the limitations thereof and how those might be overcome for conducting oxides in general.

2 Computational methodology

The Vienna *Ab initio* Simulation Package (VASP)[37–40] density functional theory (DFT) code with the projector augmented-wave (PAW) method[41] was used when calculating the structural and electronic properties of the TCOs. Convergence testing was done and an ENCUT of 450 eV was chosen for all the materials. The k-point meshes are listed in Table 3. The structures were relaxed with the Perdew–Burke–Ernzerhof[42] (PBE) for solids[43] (PBEsol) functional, as it calculates accurate solid structures while remaining computationally inexpensive.[44–46]

In order to calculate electronic transport properties, an electronic band structure and density of states (DoS) were calculated. To get accurate electronic properties, hybrid DFT with Hartree–Fock (HF) exchange[47,48] was used. These hybrid functionals yield more accurate electronic structures compared to generalised gradient approximation (GGA) functionals such as PBEsol, which tend to underestimate bandgaps.[49–64] Here, PBE0 is used for $BaSnO_3$ and SnO_2 and Heyd–Scuseria–Ernzerhof (HSE) functionals[65] were used for CdO (with 25% HF) and ZnO (with 37.5% HF) as these have been shown to work well for these TCOs.[58,66–69] The band structure and DoS were then plotted with the sumo package,[70] and the Boltzmann transport properties (BoltzTraP)[71] package was used to obtain the electrical conductivity, Seebeck coefficient and electronic thermal conductivity under the relaxation time approximation (RTA), where charge carriers are assumed to return to their ground states in a linear fashion with a lifetime of 1×10^{-14} s.

The Phonopy[72] and Phono3py[73] codes were used to calculate the vibrational properties of the TCOs. These work under the RTA like BoltzTraP, specifically under the single-mode relaxation time flavour, where each phonon mode is treated as if all the others are at equilibrium. The non-analytical correction[74] was also included, which takes into account the charges on the ions to raise the frequency of the longitudinal optic modes around the Γ point (compare ESI Fig. S3 and S4†). Phonopy and Phono3py use the supercell approach, where small displacements are created in the lattice (0.01 Å in Phonopy and 0.03 Å in Phono3py), and the forces in response to these displacements are calculated in VASP, in which the PBEsol functional was used as this has been shown to be accurate but relatively cheap for lattice dynamics calculations.[75] Phonopy uses these to calculate

Table 3 The converged k-point meshes used for most the calculations here, the denser meshes used in BoltzTraP calculations, the supercells used for the second and third order force constant calculations in Phono3py, the number of VASP calculations required to calculate the third order force constants and the q-point mesh sampled in Phono3py for BaSnO$_3$, CdO, SnO$_2$ and ZnO

| Material	BaSnO$_3$	CdO	SnO$_2$	ZnO
k-Point mesh	$5 \times 5 \times 5$	$6 \times 6 \times 6$	$3 \times 3 \times 5$	$5 \times 5 \times 3$
Dense k-points	$25 \times 25 \times 25$	$30 \times 30 \times 30$	$23 \times 23 \times 35$	$40 \times 40 \times 21$
Supercell—2nd	$6 \times 6 \times 6$	$6 \times 6 \times 6$	$4 \times 4 \times 6$	$5 \times 5 \times 4$
Supercell—3nd	$4 \times 4 \times 4$	$4 \times 4 \times 4$	$2 \times 2 \times 4$	$3 \times 3 \times 2$
Calculations—3nd	1476	442	1433	2696
q-Point mesh	$36 \times 36 \times 36$	$40 \times 40 \times 40$	$30 \times 30 \times 45$	$40 \times 40 \times 21$

second order force constants, and these were used to find supercell sizes which balanced visual convergence and computational efficiency (Table 3 and ESI Fig. S3†) to use as Phono3py inputs. Phono3py uses a much greater number of displacements to calculate the third order force constants, which can be used to calculate phonon interaction properties such as lattice thermal conductivities and the imaginary component of the self-energies per mode and per q-point. The Phono3py calculations were also completed without the RTA at 300 and 1000 K, and with and without symmetrisation of force constants, which should not result in a significant deviations in lattice thermal conductivity if the calculations are appropriate. The lattice thermal conductivities were converged against q-point mesh to ensure accurate calculations (q-points are the equivalent of k-points used in phonon calculations, $\boldsymbol{q} = 2\pi \boldsymbol{k}$). From the imaginary self-energies, the phonon lifetimes can be calculated, and from these and the group velocities, mean free paths can also be obtained:

$$\Lambda = \tau \left| \boldsymbol{v}_{\mathrm{g}} \right| \quad \text{where } \tau = \frac{1}{2\Gamma} \text{ and } \boldsymbol{v}_{\mathrm{g}} = \frac{\mathrm{d}\omega}{\mathrm{d}\boldsymbol{k}} \tag{5}$$

where Λ is the phonon mean free path, τ is the phonon lifetime, $\boldsymbol{v}_{\mathrm{g}}$ is the phonon group velocity, Γ is the imaginary component of the phonon self-energy and ω is the phonon frequency. This allows lattice thermal conductivity and its origin to be probed. Finally, an inbuilt Phono3py function was used under the RTA which limits the lifetimes of the phonons to that corresponding to a specific mean free path, here 20 nm. From this, the effects of nanostructuring on the lattice thermal conductivity of the TCOs was investigated.

3 Results

The crystal structures are shown in Fig. 1. BaSnO$_3$ has a perovskite structure, space group $Pm\bar{3}m$ (221), consisting of cubic cell of side 4.13 Å with a corner sharing SnO$_6$ octahedron at $(0, 0, 0)$ and a Ba atom at $\left(\frac{1}{2}, \frac{1}{2}, \frac{1}{2} \right)$. CdO crystallises in the rocksalt structure, space group $Fm\bar{3}m$ (225), two face-centred cubic lattices of side 4.71 Å offset by a half cell along one axis. SnO$_2$ has the rutile structure, space group $P4_2/mm$ (136), consisting of a tetragonal cell with a and b sides of 4.77 Å and c of 3.22 Å with distorted SnO$_6$ octahedra at $(0, 0, 0)$ and $\left(\frac{1}{2}, \frac{1}{2}, \frac{1}{2} \right)$, with axial
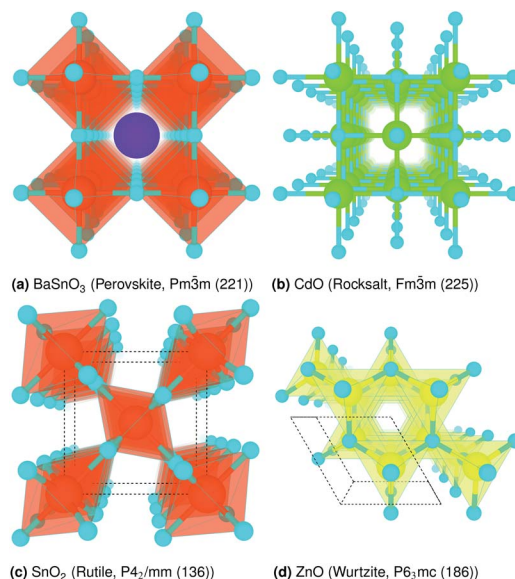

Fig. 1 Crystal structure of (a) BaSnO$_3$, (b) CdO, (c) SnO$_2$ and (d) ZnO, drawn with VESTA.[76] O is cyan, Ba purple, Sn orange, Cd lime and Zn yellow. The unit cell is drawn on (dotted lines).

bonds of 2.072 Å which form edge-sharing chains along the c axis; and equatorial bonds of 2.066 Å, which are corner-sharing in the ab planes. ZnO has the wurtzite structure, space group $P6_3mc$ (186), a hexagonal cell with a and b side lengths of 3.24 Å separated 120° perpendicular to the c direction of 5.22 Å; the atoms are arranged as corner sharing ZnO$_4$ tetrahedra of bond length 1.979 Å at $\left(\frac{1}{3}, \frac{2}{3}, 0 \right)$ and $\left(\frac{2}{3}, \frac{1}{3}, \frac{1}{2} \right)$. As BaSnO$_3$ is ternary, its more complex structure would be expected to have a reduced lattice thermal conductivity compared to the binary oxides, and hence higher ZT. Of the rest, ZnO is hexagonal, which has only twelve symmetry operations and so might be expected to have the lowest lattice thermal conductivity and hence highest ZT, followed by the tetragonal SnO$_2$ with 16 symmetry operations and cubic CdO with 48. All the structures relaxed to within 1% of their experimental lattice parameters[77–80] (ESI Table S1†).

The band structures are shown in Fig. 2. The curvature, or dispersion, of the bands indicates the mobility of charge carriers in those bands:
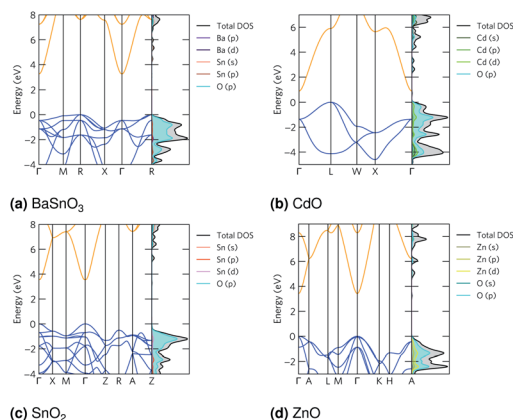
Fig. 2 The band structures, plotted with sumo[70] and using the Bradley–Cracknell formalism for k-point path nomenclature,[91] for (a) BaSnO$_3$, (b) CdO, (c) SnO$_2$ and (d) ZnO. The valence band is blue and the conduction band orange, they are normalised so the valence band maximum is at 0 eV. Expanded versions of the DoSs are available in ESI Fig. S1.†
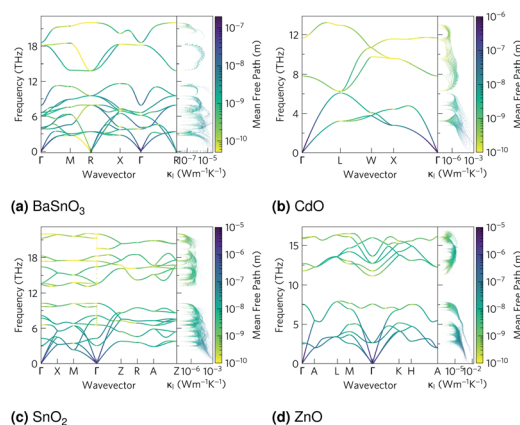

Fig. 3 The phonon dispersion relations for (a) BaSnO$_3$, (b) CdO, (c) SnO$_2$ and (d) ZnO, plotted using the Bradley–Cracknell formalism for q-point path nomenclature,[91] from which group velocity can be inferred from the band gradients. Mean free path at 1000 K is projected on the colour axis, where yellow indicates high scattering and purple indicates high mean free path. Lattice thermal conductivity (κ_l) per mode per q-point at 1000 K plotted on the right of each subfigure, sharing the frequency axis with the phonon band structure.

Table 4 Electron effective masses at the conduction band minimum and hole effective masses at the valence band maximum of BaSnO$_3$, CdO, SnO$_2$ and ZnO relative to the rest mass of an electron (m_e), evaluated by sumo[70] using parabolic band fitting

m (m_e)	BaSnO$_3$	CdO	SnO$_2$	ZnO
m_e^*	0.201 (Γ)	0.161 (Γ)	0.192 (Γ)	0.259 (Γ)
m_h^*	8.757 (M)	0.344 (L)	1.269 (Γ)	0.307 (Γ)

$$\mu = \frac{e\tau}{m^*} \quad \text{where } m^* = \frac{\hbar^2}{\left(\dfrac{d^2E}{dk^2}\right)} \tag{6}$$

where $\frac{d^2E}{dk^2}$ is the curvature of the electron bands, calculated with sumo[70] by using parabolic band fitting. All the conduction band minima (CBMs) are highly disperse, in line with previous calculations.[58,66,67,81] The electron effective masses calculated from this are in the range 0.16–0.26m_e (Table 4), which are low and therefore show a high n-type mobility in all the TCOs, so when doped they will have a high n-type conductivity, but a limited Seebeck coefficient. All give bandgaps in good agreement with experiment (Table 5).

The densities of states (DoSs) show the valence band maxima (VBMs) are dominated by O p states with some metal d and p states, particularly in CdO and ZnO. The CBMs are composed mainly of Sn, Cd or Zn s states, depending on the material, along with some O states at the CBM, particularly in CdO and ZnO. These are shown in Fig. 2, and expanded versions are in ESI Fig. S1.†

The Seebeck coefficient, electrical conductivity and electronic thermal conductivities, calculated using BoltzTraP, do not vary greatly between the TCOs (ESI Fig. S2†). The optimal ZT is often found around 1×10^{19} to 1×10^{20}, carriers per cm^3,[92] so in this work the properties are compared at 1×10^{19} carrier cm^{-3}, the lowest and therefore most achievable dopant concentration in that range. While BoltzTraP calculates the transport properties at various temperatures by artificially altering the Fermi level, and so gives no indication if these results are feasible, all these TCOs have been experimentally demonstrated to be n-type dopable above this level.[58,66,81,93–97] BaSnO$_3$, SnO$_2$ and ZnO all have relatively low Seebeck coefficients in the region of −100 to 300 μV K^{-1}, while CdO's are only around −50 to 250 μV K^{-1}. For all of them, the electrical conductivities and electronic thermal conductivities are about 100 S cm^{-1} and 0.1 W m^{-1} K^{-1} respectively.

The phonon band structures (Fig. 3, ESI Fig. S3†), calculated using Phonopy, show high dispersion as expected for such simple structures, and are therefore expected to have high lattice thermal conductivity due to a high phonon group velocity (eqn (5)). As the lattice thermal conductivity has been simulated, its origin can be analysed from the data from Phono3py. As well as the phonon band structures, Fig. 3 shows the mean free path projected on the colour axis and the contribution to

Table 5 Indirect, direct, optical and experimental bandgaps of BaSnO$_3$, CdO, SnO$_2$ and ZnO, given in eV, calculated with sumo[70]

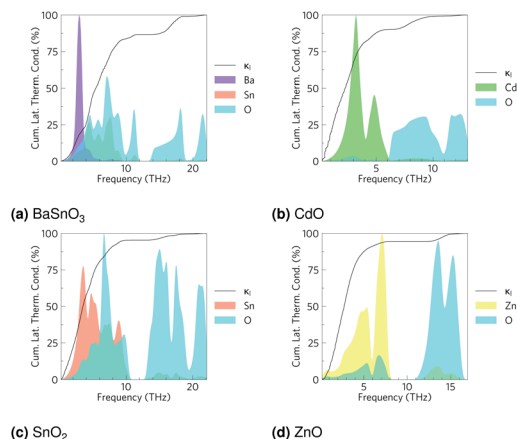| E (eV)	BaSnO$_3$	CdO	SnO$_2$	ZnO
E_g^{ind}	3.26	0.91	—	—
E_g^{dir}	3.72	2.27	3.55	3.43
$E_g^{ind,exp}$	3.1 (ref. 82–84)	0.9 (ref. 85)	—	—
$E_g^{dir,exp}$	3.4 (ref. 82)	2.4 (ref. 85)	3.56–3.59 (ref. 86–89)	3.44 (ref. 90)

Fig. 4 Cumulative lattice thermal conductivity against frequency at 1000 K in black, with the phonon density of states in arbitrary units overlaid for (a) $BaSnO_3$, (b) CdO, (c) SnO_2 and (d) ZnO.

the lattice thermal conductivity per mode per q-point on the right of each subfigure. As previously mentioned, the group velocity is high for all of them (see also ESI Fig. S5†), but we can also see the greatest mean free paths (purple) occur in the acoustic modes, and this is where the greatest contribution to the lattice thermal conductivity can be seen. One would expect the low frequency modes to be dominated by the heaviest atoms, and Fig. 4 shows that this is indeed the case for CdO, SnO_2 and ZnO, where over 60% of thermal conductivity comes from the modes below 5 THz, which are dominated by the metal cations. The relation in $BaSnO_3$ is less straightforward. ~25% of the thermal conductivity comes from below 4 THz in modes dominated by Ba, but the following ~60% comes from modes
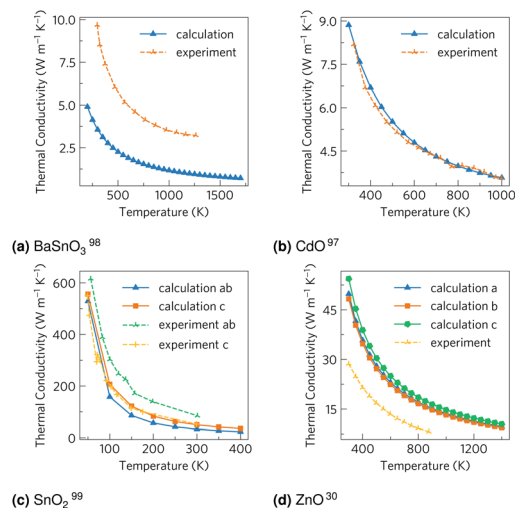

Fig. 5 The thermal conductivities calculated here and from experiment for (a) $BaSnO_3$, (b) CdO, (c) SnO_2 and (d) ZnO. For the calculations, CdO and SnO_2 use the experimental carrier concentrations of 4.2×10^{19} carriers per cm^3 and 1×10^{17} carriers per cm^3 respectively, while $BaSnO_3$ and ZnO use the arbitrary value of 1×10^{18} carriers per cm^3 as experimental data were not available. A comparison of computational methods can be seen in ESI Fig. S6.†

composed of a roughly equal mixture of Sn and O states. Overall though, one may consider reducing the phonon mean free path of the low frequency, metal dominated modes to be an effective place to start when optimising these materials.

The total thermal conductivities against temperature are shown in Fig. 5. The CdO results are in excellent agreement with experiment,[98] although the other values vary somewhat. The carrier concentrations in the experiments for $BaSnO_3$ (ref. 99) and ZnO[31] were not reported, so the arbitrary value of 1×10^{18} carriers cm^{-3} used here could help explain some the discrepancy, although the differences are out of the range of the effect of modulating the electron concentration, so there are certainly other factors at play. It should be noted the experimental measurements on CdO, $BaSnO_3$ and ZnO were taken on powdered samples rather than single crystals as with SnO_2, which would scatter phonons at the 'grain' boundaries, reducing the thermal conductivity and averaging anisotropic conduction. Nevertheless, when comparing our unsymmetrised RTA results with those computed without RTA and those where the force constants have been symmetrised, we found the agreement to be excellent (ESI Fig. S6†).

Using the lattice thermal conductivity from Phono3py and the electronic transport properties from BoltzTraP, the ZT was calculated. Maximum ZTs occur at high doping concentrations of $\sim 1 \times 10^{19}$ carriers per cm^3 for $BaSnO_3$, $\sim 2 \times 10^{19}$ carriers per cm^3 for CdO, $\sim 3 \times 10^{19}$ carriers per cm^3 for SnO_2 and $\sim 8 \times 10^{19}$ carriers per cm^3 for ZnO. In order for a material to be an efficient thermoelectric, it must also be a degenerate conductor, *i.e.* display metal-like conduction, which occurs for carrier concentrations above the Mott criterion, n_{Mott}:[61,100,101]

$$n_{Mott} > \left(\frac{0.26}{a_0}\right)^3 \quad \text{where} \quad a_0 = \frac{4\pi\varepsilon_0\hbar^2}{m^*e^2} \quad \text{and} \quad \frac{1}{m^*} = \frac{1}{m_e^*} + \frac{1}{m_h^*} \quad (7)$$

where a_0 is the effective Bohr radius and ε_0 is the static dielectric constant, the sum of the ionic and high frequency components, ε_{ion} and ε_∞, respectively. All the TCOs reach their highest ZTs above their Mott criteria (Table 6), and all have previously been shown to be highly dopable,[58,66,81,93–97] so all can feasibly achieve their maximum ZT. Nevertheless, the maximum ZTs are not high, even at temperatures close to their melting or decomposition points (Table 2), CdO, SnO_2 and ZnO have ZTs of around 0.5. $BaSnO_3$ approaches a ZT of 2, but only at very high temperatures of around 1700 K (Fig. 6).

Table 6 Ionic (ε_{ion}) and high frequency (ε_∞) contributions to the relative static dielectric constant, ε_0, the effective Bohr radius, a_0 and the Mott criterion, n_{Mott}, the carrier concentration above which the material becomes a degenerate conductor, calculated from eqn (7), for $BaSnO_3$, CdO, SnO_2 and ZnO

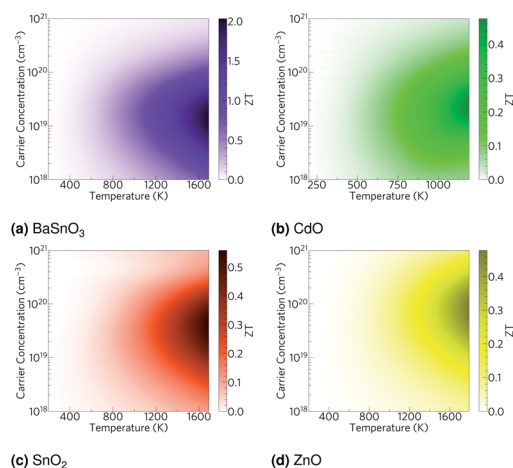| Material	$BaSnO_3$	CdO	SnO_2	ZnO
ε_{ion}	15.4	11.6	7.6	4.7
ε_∞	3.4	4.3	2.5	2.8
ε_0	18.8	15.9	10.1	7.5
a_0 (m)	5.06×10^{-9}	7.67×10^{-9}	3.20×10^{-9}	2.83×10^{-9}
n_{Mott} (cm^{-3})	1.35×10^{17}	3.89×10^{16}	5.34×10^{17}	7.79×10^{17}

Fig. 6 Heat maps of the *ZT* against carrier concentration and temperature for (a) BaSnO$_3$, (b) CdO, (c) SnO$_2$ and (d) ZnO. The values are averaged over crystal orientation for SnO$_2$ and ZnO as any real devices would need to be heavily nanostructured.

4 Discussion

All the materials studied here have broadly comparable Seebeck coefficients, electrical conductivities and electronic thermal conductivities (Table 7). They have neither the combined high Seebeck coefficient and high electrical conductivity of AgPb$_{18}$-SbTe$_{20}$ nor the low thermal conductivity of SnSe. Electrical conductivity is easily increased by doping, increasing carrier concentration at the cost of Seebeck coefficient, but a much more interesting way is band engineering. Alloying Mg$_3$Sb$_2$ with Mg$_3$Bi$_2$ barely reduces the Seebeck coefficient, despite an increase in the curvature of the bands,[102] probably due to an increased number of bands at the conduction band minimum, resulting in a higher density of states there and hence raising the Seebeck coefficient nearly as much as it is lowered by the lower effective mass. That said, in the TCOs the CBMs are several eV lower than the rest of the conduction bands, so band engineering in the same way as the Mg$_3$(Sb,Bi)$_2$ system is almost certainly impossible.

This leaves reducing the lattice thermal conductivity as the only option for improving the TCOs' thermoelectric efficiency. This is the quantity that varies most between the TCOs and hence
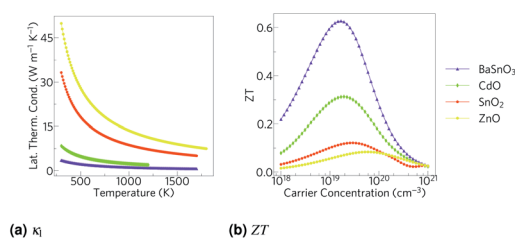

Fig. 7 (a) The lattice thermal conductivity, κ_l, against temperature and (b) the *ZT* calculated from Phono3py and BoltzTraP against carrier concentration for BaSnO$_3$, CdO, SnO$_2$ and ZnO at 1000 K.

is the determining factor in the relative magnitude of their *ZT*s (Fig. 7). This demonstrates that the power factor, as is sometimes used as an alternative screening metric for *ZT* when the lattice thermal conductivity has not been measured or calculated, is not a sufficient measure of the thermoelectric efficiency of these materials. As we predicted, the ternary BaSnO$_3$ has the lowest lattice thermal conductivity, likely due to its comparative structural complexity. As it has two cations, we also considered the effect of Ba$_{Sn}$–Sn$_{Ba}$ antisite pairs, but found the energy too high for a significant proportion of defects to be present (ESI Table S2†). In the binary systems, symmetry was not a good predictor of the lattice thermal conductivities of the remaining TCOs as was proposed. The high lattice thermal conductivity of ZnO can be at least partially explained by the relatively small mass difference between Zn and O, which would mean phonons can more easily transfer between the atoms. Similar reasoning cannot be applied to CdO and SnO$_2$, perhaps because the effect of the small 6.3 amu mass difference between Cd and Sn, as opposed to the almost 50 amu difference between Zn and Cd, is small compared to other effects such as that of the bonding.

As we have calculated the lattice thermal conductivity *ab initio*, we have been further able to analyse its origin and hence how it can be minimised. The highest contributions to the lattice thermal conductivity occur in the metal-dominated acoustic modes, where the mean free paths are long, and the materials with the longest mean free paths are the ones with highest lattice thermal conductivities. While the low frequency modes being metal dominated may suggest changing the cations would be the optimal way to reduce the lattice thermal conductivity, this is not necessarily true, as the strength of the

Table 7 Seebeck coefficient, α, electrical conductivity, σ, electronic and lattice contributions to the thermal conductivity, κ_e and κ_l and *ZT* for BaSnO$_3$, CdO, SnO$_2$ and ZnO studied here and approximate quantities for SnSe[12] and AgPb$_{18}$SbTe$_{20}$.[9] Only the total thermal conductivity was available for AgPb$_{18}$SbTe$_{20}$. All quantities are at 800 K. The TCOs' and SnSe's carrier concentrations are 1×10^{19} carriers per cm^3 and AgPb$_{18}$SbTe$_{20}$'s is 2.15×10^{19} carriers per cm^3

Material	α (μV K^{-1})	σ (S cm^{-1})	κ_e (W m^{-1} K^{-1})	κ_l (W m^{-1} K^{-1})	*ZT*
BaSnO$_3$	−230	127	0.188	1.43	0.348
CdO	−204	150	0.234	2.97	0.169
SnO$_2$	−243	159	0.198	13.0	0.0628
ZnO	−203	95.2	0.143	17.4	0.0402
SnSe (ref. 12)	350	100	0.05	0.3	1.9
AgPb$_{18}$SbTe$_{20}$ (ref. 9)	−370	200	1.1		2.1

bonds also contributes to the lattice thermal conductivity. The fact that in $BaSnO_3$ and SnO_2 there are significant amounts of O in the low frequency modes suggests that altering the anions could also alter the characteristics of the low frequency modes, one would imagine especially if the anion were heavy and hence would vibrate at a relatively low frequency. One way reduce the mean free paths is to chemically alter the material, *e.g.* by ion mutation, where, for example, a 2+ ion could be replaced with 50% each of a 1+ and 3+ ion. If these ions are different sizes, the mass variation could cause more phonon scattering.[103] Alternatively, a commonly used physical method is nanostructuring, physically blocking long mean free path phonons with grain boundaries. To get an indication of how effective this might be in the TCOs, the cumulative lattice thermal conductivity was plotted against mean free path (Fig. 8). Hsu *et al.*[9] nanostructured $AgPb_{18}SbTe_{20}$ down to 20–30 nm to restrict phonon mean free paths and hence reduce the lattice thermal conductivity and increase *ZT* from ~0.5 (ref. 104) to 2.2. At 1000 K, whilst only about 7% of the lattice thermal conductivity in $BaSnO_3$ is from phonons which have mean free paths greater than 20 nm, CdO has 63% of its lattice thermal conductivity from phonons above this threshold, SnO_2 has 86% and ZnO has 92% from phonons greater than 20 nm (Fig. 8). This suggests that nanostructuring may have a significant effect on the lattice thermal conductivity of CdO and especially SnO_2 and ZnO, although it would also be expected to negatively effect the electrical conductivity and alter other properties as well, and it would likely preclude the TCOs from being *transparent* thermoelectrics due to grain boundaries scattering light. It has previously been reported, however, that boundaries can affect lattice thermal conductivity more than electrical conductivity,[105] so considering only the influence on lattice thermal conductivity is not completely unfounded. Mean free path as a cause of

low lattice thermal conductivity makes sense in the context of the rest of the results: $BaSnO_3$ is the only ternary studied here, and the complexity arising from this means its mean free paths are shorter, which leads to a lower thermal conductivity and hence higher *ZT*. In_2O_3 is an example of another complex-structured TCO, which has 40 atoms per cell as opposed to the 2–6 in the materials studied here. It has the highest singly doped *ZT* for a TCO of 0.45 at 1273 K, attributed in part to thermal conductivities lower than the experimental results referenced here.[24,99] A further example of structural complexity increasing *ZT* is dual Ga and Al doped ZnO,[23] which achieved a *ZT* of 0.65, the highest for a TCO. Here, the maximum n-type *ZT* for single-crystal ZnO is 0.077 at 1000 K, which Ohtaki *et al.* improved by over eight times by co-doping.

By reducing the phonon lifetimes of long mean free path phonons so the mean free path is limited to a maximum of 20 nm, the level of nanostructuring achieved by Hsu *et al.*,[9] the effect of nanostructuring on each material studied here is predicted. Note this is assuming all the other properties of the materials remain the same, which is unrealistic. It furthermore assumes that the actual interactions of the dopants are negligible, although as is clear from the dually Ga and Al doped ZnO these interactions can cause significant *ZT* enhancements. Nevertheless, this should give an indication of the relative effects. Under this approximation, shown in Fig. 9, $BaSnO_3$ remains the highest efficiency thermoelectric with a barely increased *ZT* of 2, but due to their significant phonon mean free paths, CdO, SnO_2 and ZnO increase in *ZT*, with the *ZT* of ZnO more than doubling (Table 8). Overall, $BaSnO_3$ shows promise as a high temperature thermoelectric, reaching a *ZT* of 2 at 1700 K even without nanostructuring, and the naturally low mean free paths make it anyway pointless to nanostructure. Of the remainder, CdO shows least promise due to the dual factors of its relatively low decomposition temperature and relatively short mean free paths, reaching an approximated nano-structured *ZT* of about 0.6 at 1200 K. With their long mean free
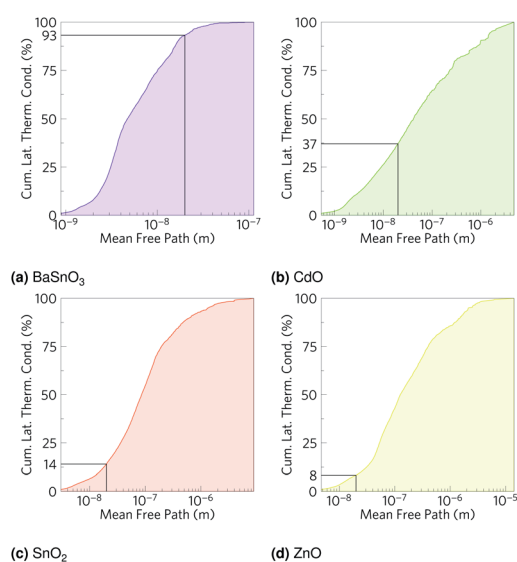

Fig. 8 Cumulative lattice thermal conductivity against phonon mean free path for (a) $BaSnO_3$, (b) CdO, (c) SnO_2 and (d) ZnO at 1000 K. The percentage of phonons of mean free path less than 20 nm is marked on.
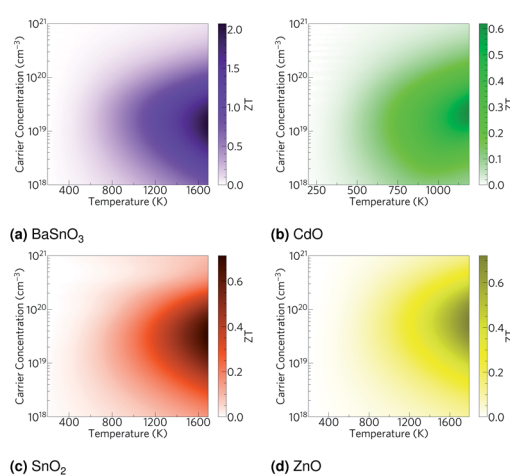

Fig. 9 Heat maps of the *ZT* against carrier concentration and temperature, excluding the phonons of mean free path greater than 20 nm to approximate the effect of nanostructuring, for (a) $BaSnO_3$, (b) CdO, (c) SnO_2 and (d) ZnO.

Table 8 The lattice thermal conductivity of the single crystal, κ_l, the ratio of phonons with mean free paths less than 20 nm and the lattice thermal conductivity with the mean free paths of these phonons limited to 20 nm, $\kappa_{l,nano}$. Then, the maximum single crystal ZT calculated here, ZT_{max}, the ZT with the mean free path limited lattice thermal conductivity, $ZT_{max,nano}$, and the enhancement factor of nanostructuring at 1000 K. These are computed for each of BaSnO$_3$, CdO, SnO$_2$ and ZnO, using as reference the study of Hsu et al.[9]

Material	BaSnO$_3$	CdO	SnO$_2$	ZnO
κ_l (W m^{-1} K^{-1})	1.18	2.35	9.29	15.0
Phonons $\leq$ 20 nm (%)	92	38	17	8
$\kappa_{l,nano}$ (W m^{-1} K^{-1})	1.08	1.51	4.90	6.22
ZT_{max}	0.62	0.31	0.13	0.077
$ZT_{max,nano}$	0.65	0.45	0.21	0.17
Enhancement factor (%)	105	145	162	221

paths, SnO$_2$ and ZnO show a greater effectiveness of nanostructuring, reaching ZTs of around 0.7 at temperatures around 1700 K, although at a given temperature they have lower ZTs than CdO. It must be stressed that these are rough approximations, omitting the effects of nanostructuring and specific dopants or combinations thereof on electronic properties, but it does help explain the significant improvements that have been made experimentally in ZnO by nanostructuring, and proposes nanostructuring SnO$_2$ may be similarly effective.

As mean free paths not only predict the thermal conductivity, and therefore ZT of these TCOs, but also determine to what extent they can be improved by nanostructuring, this research shows that the only way we can truly tell which oxides will be the most effective targets for thermoelectric materials is by fully simulating the phononic interactions, in order to predict the mean free paths.

5 Conclusions

Here we have used hybrid density functional theory and GGA lattice dynamics to analyse the origin of the thermoelectric performance of four TCOs: BaSnO$_3$, CdO, SnO$_2$ and ZnO. We have found that phonon mean free path is the defining factor in the thermoelectric efficiency of these materials, and that nanostructuring could offer significant improvements to those materials with the longest mean free paths. Due to its naturally low mean free paths, BaSnO$_3$ has been predicted to be able to exceed a ZT of 2 at 1700 K, regardless of nanostructuring. Despite unremarkable ZTs reaching only about 0.5 at 1700 K without nanostructuring, as large portions of SnO$_2$ and ZnO's lattice thermal conductivities come from long mean free path phonons, these values could potentially be increased to 0.7 with large degrees of nanostructuring. We have shown that a thorough theoretical analysis of the lattice thermal conductivity is necessary to understand how to optimise conducting oxides for thermoelectric applications.

Conflicts of interest

There are no conflicts to declare.

References

1 S. Kan, B. Chen and G. Chen, *Appl. Energy*, 2019, **250**, 1235.

2 U. Soytaş, R. Sarı, *Routledge Handbook of Energy Economics*, Routledge, 2019.

3 C. Mora, D. Spirandelli, E. C. Franklin, J. Lynham, M. B. Kantar, W. Miles, C. Z. Smith, K. Freel, J. Moy, L. V. Louis, E. W. Barba, K. Bettinger, A. G. Frazier, J. F. Colburn IX, N. Hanasaki, E. Hawkins, Y. Hirabayashi, W. Knorr, C. M. Little, K. Emanuel, J. Sheffield, J. A. Patz and C. L. Hunter, *Nat. Clim. Change*, 2018, **8**, 1062.

4 A. Firth, B. Zhang and A. Yang, *Appl. Energy*, 2019, **235**, 1314.

5 R. D. Bornstein, *J. Appl. Meteorol.*, 1968, **7**, 575.

6 T. J. Seebeck, in *Abhandlungen der Königlich Preussischen Akademie der Wissenschaften*, Deutsche Akademie der Wissenschaften zu Berlin, Berlin, 1st edn, 1825, pp. 265–373.

7 R. Franz and G. Wiedemann, *Ann. Phys.*, 1853, **165**, 497.

8 G. A. Slack, in *CRC Handbook of Thermoelectrics*, ed. D. M. Rowe, CRC Press, Boca Raton, 1st edn, 1995, ch. 34, pp. 407–440.

9 K. F. Hsu, S. Loo, F. Guo, W. Chen, J. S. Dyck, C. Uher, T. Hogan, E. K. Polychroniadis and M. G. Kanatzidis, *Science*, 2004, **303**, 818.

10 K. Biswas, J. He, I. D. Blum, C.-I. Wu, T. P. Hogan, D. N. Seidman, V. P. Dravid and M. G. Kanatzidis, *Nature*, 2012, **489**, 414.

11 R. J. Korkosz, T. C. Chasapis, S.-h. Lo, J. W. Doak, Y. J. Kim, C.-I. Wu, E. Hatzikraniotis, T. P. Hogan, D. N. Seidman, C. Wolverton, V. P. Dravid and M. G. Kanatzidis, *J. Am. Chem. Soc.*, 2014, **136**, 3225.

12 L.-D. Zhao, S.-H. Lo, Y. Zhang, H. Sun, G. Tan, C. Uher, C. Wolverton, V. P. Dravid and M. G. Kanatzidis, *Nature*, 2014, **508**, 373.

13 H. J. Wu, L.-D. Zhao, F. S. Zheng, D. Wu, Y. L. Pei, X. Tong, M. G. Kanatzidis and J. Q. He, *Nat. Commun.*, 2014, **5**, 4515.

14 T. Fu, X. Yue, H. Wu, C. Fu, T. Zhu, X. Liu, L. Hu, P. Ying, J. He and X. Zhao, *Journal of Materiomics*, 2016, **2**, 141.

15 S. Carnot, *Réflexions sur la Puissance Motrice du Feu et sur les Machines Propres à Développer Cette Puissance*, Bachelier, 1824.

16 S. Carnot and W. Thompson, *Reflections on the Motive Power of Heat*, John Wiley & Sons, 1897.

17 K. Koumoto, I. Terasaki and R. Funahashi, *MRS Bull.*, 2006, **31**, 206.

18 G. Wagner and H. Binder, *Z. Anorg. Allg. Chem.*, 1958, **297**, 328.

19 F. Sibieude, M. Ducarroir, A. Tofighi and J. Ambriz, *Int. J. Hydrogen Energy*, 1982, **7**, 79.

20 *CRC Handbook of Chemistry and Physics*, ed. J. R. Rumble Jr, D. R. Lide and T. J. Bruno, CRC Press, 98th edn, 2017.

21 M. Ohtaki, T. Tsubota, K. Eguchi and H. Arai, *J. Appl. Phys.*, 1996, **79**, 1816.

22 J. Loureiro, N. Neves, R. Barros, T. Mateus, R. Santos, S. Filonovich, S. Reparaz, C. M. Sotomayor-Torres, F. Wyczisk, L. Divay, R. Martins and I. Ferreira, *J. Mater. Chem. A*, 2014, **2**, 6649.

23 M. Ohtaki, K. Araki and K. Yamamoto, *J. Electron. Mater.*, 2009, **38**, 1234.

24 D. Bérardan, E. Guilmeau, A. Maignan and B. Raveau, *Solid State Commun.*, 2008, **146**, 97.

25 L. Li, L. Fang, X. M. Chen, J. Liu, F. F. Yang, Q. J. Li, G. B. Liu and S. J. Feng, *Phys. E*, 2008, **41**, 169.

26 D. Bérardan, C. Byl and N. Dragoe, *J. Am. Ceram. Soc.*, 2010, **93**, 2352.

27 P. Mele, S. Saini, H. Honda, K. Matsumoto, K. Miyazaki, H. Hagino and A. Ichinose, *Appl. Phys. Lett.*, 2013, **102**, 253903.

28 L. Han, N. Van Nong, L. T. Hung, T. Holgate, N. Pryds, M. Ohtaki and S. Linderoth, *J. Alloys Compd.*, 2013, **555**, 291.

29 L. Li, L. Fang, X. J. Zhou, Z. Y. Liu, L. Zhao and S. Jiang, *J. Electron Spectrosc. Relat. Phenom.*, 2009, **173**, 7.

30 T. Tsubota, M. Ohtaki, K. Eguchi and H. Arai, *J. Mater. Chem.*, 1997, **7**, 85.

31 K. Cai, E. Müller, C. Drašar and A. Mrotzek, *Mater. Sci. Eng., B*, 2003, **104**, 45.

32 H. Cheng, X. J. Xu, H. H. Hng and J. Ma, *Ceram. Int.*, 2009, **35**, 3067.

33 N. Ma, J.-F. Li, B. P. Zhang, Y. H. Lin, L. R. Ren and G. F. Chen, *J. Phys. Chem. Solids*, 2010, **71**, 1344.

34 X. Qu, W. Wang, S. Lv and D. Jia, *Solid State Commun.*, 2011, **151**, 332.

35 P. Fan, Y.-z. Li, Z.-h. Zheng, Q.-y. Lin, J.-t. Luo, G.-x. Liang, M.-q. Zhang and M.-c. Chen, *Appl. Surf. Sci.*, 2013, **284**, 145.

36 P. Jood, R. J. Mehta, Y. Zhang, G. Peleckis, X. Wang, R. W. Siegel, T. Borca-Tasciuc, S. X. Dou and G. Ramanath, *Nano Lett.*, 2011, **11**, 4337.

37 G. Kresse and J. Hafner, *Phys. Rev. B: Condens. Matter Mater. Phys.*, 1993, **48**, 13115.

38 G. Kresse and J. Hafner, *Phys. Rev. B: Condens. Matter Mater. Phys.*, 1993, **47**, 558.

39 G. Kresse and J. Hafner, *J. Phys.: Condens. Matter*, 1994, **6**, 8245.

40 G. Kresse and J. Furthmüller, *Comput. Mater. Sci.*, 1996, **6**, 15.

41 P. E. Blöchl, *Phys. Rev. B: Condens. Matter Mater. Phys.*, 1994, **50**, 17953.

42 J. P. Perdew, K. Burke and M. Ernzerhof, *Phys. Rev. Lett.*, 1996, **77**, 3865.

43 J. P. Perdew, A. Ruzsinszky, G. I. Csonka, O. A. Vydrov, G. E. Scuseria, L. A. Constantin, X. Zhou and K. Burke, *Phys. Rev. Lett.*, 2008, **100**, 136406.

44 G. M. D. Nguimdo and D. P. Joubert, *Eur. Phys. J. B*, 2015, **88**, 113.

45 M. De La Pierre, R. Orlando, L. Maschio, K. Doll, P. Ugliengo and R. Dovesi, *J. Comput. Chem.*, 2011, **32**, 1775.

46 L. He, F. Liu, G. Hautier, M. J. T. Oliveira, M. A. Marques, F. D. Vila, J. J. Rehr, G.-M. Rignanese and A. Zhou, *Phys. Rev. B: Condens. Matter Mater. Phys.*, 2014, **89**, 064305.

47 D. R. Hartree, *Math. Proc. Cambridge Philos. Soc.*, 1928, **24**, 89.

48 V. Fock, *Z. Phys. A*, 1930, **61**, 126.

49 J. Heyd and G. E. Scuseria, *J. Chem. Phys.*, 2004, **121**, 1187.

50 J. Heyd, J. E. Peralta, G. E. Scuseria and R. L. Martin, *J. Chem. Phys.*, 2005, **123**, 174101.

51 S. Chen, X. G. Gong, A. Walsh and S.-H. Wei, *Appl. Phys. Lett.*, 2009, **94**, 041903.

52 B. G. Janesko, T. M. Henderson and G. E. Scuseria, *Phys. Chem. Chem. Phys.*, 2009, **11**, 443.

53 D. O. Scanlon, B. J. Morgan, G. W. Watson and A. Walsh, *Phys. Rev. Lett.*, 2009, **103**, 096405.

54 A. Stroppa and G. Kresse, *Phys. Rev. B: Condens. Matter Mater. Phys.*, 2009, **79**, 201201.

55 J. P. Allen, D. O. Scanlon and G. W. Watson, *Phys. Rev. B: Condens. Matter Mater. Phys.*, 2010, **81**, 161103.

56 F. Oba, M. Choi, A. Togo, A. Seko and I. Tanaka, *J. Phys.: Condens. Matter*, 2010, **22**, 384211.

57 A. Stroppa and S. Picozzi, *Phys. Chem. Chem. Phys.*, 2010, **12**, 5405.

58 M. Burbano, D. O. Scanlon and G. W. Watson, *J. Am. Chem. Soc.*, 2011, **133**, 15065.

59 P. Deák, B. Aradi and T. Frauenheim, *Phys. Rev. B: Condens. Matter Mater. Phys.*, 2011, **83**, 155207.

60 A. B. Kehoe, D. O. Scanlon and G. W. Watson, *Phys. Rev. B: Condens. Matter Mater. Phys.*, 2011, **83**, 233202.

61 D. O. Scanlon, A. B. Kehoe, G. W. Watson, M. O. Jones, W. I. F. David, D. J. Payne, R. G. Egdell, P. P. Edwards and A. Walsh, *Phys. Rev. Lett.*, 2011, **107**, 246402.

62 D. O. Scanlon and G. W. Watson, *J. Mater. Chem.*, 2011, **21**, 3655.

63 A. Walsh, S. Chen, S.-H. Wei and X.-G. Gong, *Adv. Energy Mater.*, 2012, **2**, 400.

64 D. Fritsch, B. J. Morgan and A. Walsh, *Nanoscale Res. Lett.*, 2017, **12**, 19.

65 J. Heyd, G. E. Scuseria and M. Ernzerhof, *J. Chem. Phys.*, 2003, **118**, 8207.

66 D. O. Scanlon, *Phys. Rev. B: Condens. Matter Mater. Phys.*, 2013, **87**, 161201.

67 D. O. Scanlon and G. W. Watson, *J. Mater. Chem.*, 2012, **22**, 25236.

68 A. M. Ganose and D. O. Scanlon, *J. Mater. Chem. C*, 2016, **4**, 1467.

69 F. Oba, A. Togo, I. Tanaka, J. Paier and G. Kresse, *Phys. Rev. B: Condens. Matter Mater. Phys.*, 2008, **77**, 245202.

70 A. M. Ganose, A. J. Jackson and D. O. Scanlon, *J. Open Source Softw.*, 2018, **3**, 717.

71 G. K. H. Madsen and D. J. Singh, *Comput. Phys. Commun.*, 2006, **175**, 67.

72 A. Togo and I. Tanaka, *Scr. Mater.*, 2015, **108**, 1.

73 A. Togo, L. Chaput and I. Tanaka, *Phys. Rev. B: Condens. Matter Mater. Phys.*, 2015, **91**, 094306.

74 X. Gonze, J.-C. Charlier, D. C. Allan and M. P. Teter, *Phys. Rev. B: Condens. Matter Mater. Phys.*, 1994, **50**, 13035.

75 J. M. Skelton, D. Tiana, S. C. Parker, A. Togo, I. Tanaka and A. Walsh, *J. Chem. Phys.*, 2015, **143**, 064710.

76 K. Momma and F. Izumi, *J. Appl. Crystallogr.*, 2011, **44**, 1272.

77 G. A. Geguzina and V. P. Sakhnenko, *Crystallogr. Rep.*, 2004, **49**, 15.

78 H. Singh and B. Dayal, *Solid State Commun.*, 1969, **7**, 725.

79 R. L. Clendenen and H. G. Drickamer, *J. Chem. Phys.*, 1966, **44**, 4223.

80 R. R. Reeber, *J. Appl. Phys.*, 1970, **41**, 5063.

81 S. C. Dixon, S. Sathasivam, B. A. D. Williamson, D. O. Scanlon, C. J. Carmalt and I. P. Parkin, *J. Mater. Chem. C*, 2017, **5**, 7585.

82 G. Larramona, C. Gutiérrez, I. Pereira, M. R. Nunes and F. M. da Costa, *J. Chem. Soc., Faraday Trans. 1*, 1989, **85**, 907.

83 H. Mizoguchi, H. W. Eng and P. M. Woodward, *Inorg. Chem.*, 2004, **43**, 1667.

84 W. Zhang, J. Tang and J. Ye, *J. Mater. Res.*, 2007, **22**, 1859.

85 I. N. Demchenko, J. D. Denlinger, M. Chernyshova, K. M. Yu, D. T. Speaks, P. Olalde-Velasco, O. Hemmers, W. Walukiewicz, A. Derkachova and K. Lawniczak-Jablonska, *Phys. Rev. B: Condens. Matter Mater. Phys.*, 2010, **82**, 075107.

86 M. Nagasawa and S. Shionoya, *Phys. Lett.*, 1966, **22**, 409.

87 D. Fröhlich, R. Kenklies and R. Helbig, *Phys. Rev. Lett.*, 1978, **41**, 1750.

88 K. Reimann and M. Steube, *Solid State Commun.*, 1998, **105**, 649.

89 M. Feneberg, C. Lidig, K. Lange, R. Goldhahn, M. D. Neumann, N. Esser, O. Bierwagen, M. E. White, M. Y. Tsai and J. S. Speck, *Appl. Phys. Lett.*, 2014, **104**, 231106.

90 W. Y. Liang and A. D. Yoffe, *Phys. Rev. Lett.*, 1968, **20**, 59.

91 C. Bradley and A. Cracknell, *The Mathematical Theory of Symmetry in Solids: Representation Theory for Point Groups and Space Groups*, Oxford University Press, 2009.

92 G. J. Snyder and E. S. Toberer, *Nat. Mater.*, 2008, **7**, 105.

93 A. K. Singh, A. Janotti, M. Scheffler and C. G. Van de Walle, *Phys. Rev. Lett.*, 2008, **101**, 055502.

94 P. Ágoston, C. Körber, A. Klein, M. J. Puska, R. M. Nieminen and K. Albe, *J. Appl. Phys.*, 2010, **108**, 053511.

95 A. Janotti and C. G. Van de Walle, *Phys. Rev. B: Condens. Matter Mater. Phys.*, 2007, **76**, 165202.

96 J. E. N. Swallow, B. A. D. Williamson, T. J. Whittles, M. Birkett, T. J. Featherstone, N. Peng, A. Abbott, M. Farnworth, K. J. Cheetham, P. Warren, D. O. Scanlon, V. R. Dhanak and T. D. Veal, *Adv. Funct. Mater.*, 2018, **28**, 1701900.

97 M. J. Powell, B. A. D. Williamson, S.-Y. Baek, J. Manzi, D. B. Potter, D. O. Scanlon and C. J. Carmalt, *Chem. Sci.*, 2018, **9**, 7968.

98 L. Li, S. Liang, S. Li, J. Wang, S. Wang, G. Dong and G. Fu, *Nanotechnology*, 2014, **25**, 425402.

99 T. Maekawa, K. Kurosaki and S. Yamanaka, *J. Alloys Compd.*, 2006, **416**, 214.

100 N. Mott, *Rev. Mod. Phys.*, 1968, **40**, 677.

101 P. P. Edwards and M. J. Sienko, *Phys. Rev. B: Condens. Matter Mater. Phys.*, 1978, **17**, 2575.

102 J. Zhang and B. B. Iversen, *J. Appl. Phys.*, 2019, **126**, 085104.

103 T. Shibuya, J. M. Skelton, A. J. Jackson, K. Yasuoka, A. Togo, I. Tanaka and A. Walsh, *APL Mater.*, 2016, **4**, 104809.

104 Y.-L. Pei and Y. Liu, *J. Alloys Compd.*, 2012, **514**, 40.

105 M. S. Dresselhaus, G. Chen, M. Y. Tang, R. G. Yang, H. Lee, D. Z. Wang, Z. F. Ren, J.-P. Fleurial and P. Gogna, *Adv. Mater.*, 2007, **19**, 1043.